IOP Publishing Journal of Physics D: Applied Physics
J. Phys. D: Appl. Phys. **40** (2007) 5917–5923 doi:10.1088/0022-3727/40/19/021

Spectroscopic diagnostics of plasma during laser processing of aluminium

R Lober[1] **and J Mazumder**[2,3]

[1] Sandia National Laboratories, PO Box 5800, Albuquerque, NM 87185-MS0841, USA
[2] Center for Laser Aided Intelligent Manufacturing, Room 2040, G G Brown Laboratory, 2350 Hayward Street, University of Michigan, Ann Arbor, MI 48109-2125, USA

E-mail: mazumder@umich.edu and rrlober@sandia.gov

Received 14 February 2007, in final form 19 June 2007
Published 21 September 2007
Online at stacks.iop.org/JPhysD/40/5917

Abstract
The role of the plasma in laser–metal interaction is of considerable interest due to its influence in the energy transfer mechanism in industrial laser materials processing. A 10 kW CO_2 laser was used to study its interaction with aluminium under an argon environment. The objective was to determine the absorption and refraction of the laser beam through the plasma during the processing of aluminium. Laser processing of aluminium is becoming an important topic for many industries, including the automobile industry. The spectroscopic relative line to continuum method was used to determine the electron temperature distribution within the plasma by investigating the 4158 Å Ar I line emission and the continuum adjacent to it. The plasmas are induced in 1.0 atm pure Ar environment over a translating Al target, using $f/7$ and 10 kW CO_2 laser. Spectroscopic data indicated that the plasma composition and behaviour were Ar-dominated. Experimental results indicated the plasma core temperature to be 14 000–15 300 K over the incident range of laser powers investigated from 5 to 7 kW. It was found that 7.5–29% of the incident laser power was absorbed by the plasma. Cross-section analysis of the melt pools from the Al samples revealed the absence of any key-hole formation and confirmed that the energy transfer mechanism in the targets was conduction dominated for the reported range of experimental data.

1. Introduction

Commercial use of high power CW lasers has increased significantly since the invention of the device nearly three decades ago. Welding and surface modification of Al alloys are important industrial applications. Due to the low melting point of Al and high reflectivity, interaction with CW laser has become an interesting challenge. The laser beam intensity at the surface for Al processing is often high enough for plasma to form. This plasma consists of vaporized material and ionized ambient gas. One interesting side effect of the plasma is the enhanced or reduced coupling, which can take place when flux in the order of 10^8 W cm^{-2} or greater is achieved. There is considerable debate in the literature over the nature of the coupling, which occurs. Reduced coupling occurs due to the beam absorption within the plasma column or possible reflection of the beam from the plasma itself. The reflectivity of the plasma increases when metallic components of the plasma increase. The absorption within the plasma is a function of the electron number density of the plasma. This paper describes an experimental investigation on Al/Ar plasmas over a range of laser power and translation speed, which may be of interest to various laser applications including cutting, welding and surface modification.

Various researchers have studied plasma for laser/Al interaction. Knudtson *et al* [1] used both spatial and temporal resolution to record the emission spectrum of an Al laser induced plasma (LIP) within a vacuum chamber at 10^{-2} Torr. A flash lamp pumped dye laser was employed to deliver intensities of up to 5×10^7 W cm^{-2} to the aluminum target.

[3] Author to whom any correspondence should be addressed.

The gated optical multi-channel analyser (OMA) was used to observe the LIP at various delay times with respect to the leading edge of the laser pulse and at various distances away from the surface. Almost all the aluminum lines arose from the Al II and Al III except for a resonance doublet (Al I) at 394.4 and 396.1 nm. Since it was assumed that the local thermodynamic equilibrium (LTE) was valid, the electron temperature was calculated from the relative line emissivities of the given ionization state. The electron temperature ranged from 7.66 ± 0.31 to $8.31 \pm 0.54 \times 10^3$ K. The electron density measurement was performed on four well-defined Al II lines for which the stark broadening coefficient had previously been measured. The electron densities ranged from 1.1 ± 1.4 to $7.7 \pm 2.1 \times 10^{17}$ cm^{-3} with an average of 4.4×10^{17} cm^{-3}. The spatial dependence on the electron temperature is recorded to be virtually constant (7000–8000 K), from the surface out to 7 mm away, while the electron density decreases by an order of magnitude. The transient data indicated a tendency of the temperature to 'clamp' to a value of approximately 8000 K from early in the rise of the pulse up to the pulse tail at 3 mm. No well-resolved Al III lines were observed. To conclude, the electron temperature and the density of the Al LIP was successfully resolved as a function of time and space for incident fluxes up to 5×10^7 W cm^{-2}. It was theorized that the same technique would be applicable to higher incident laser fluxes.

McKay *et al* [2] investigated the thermal response of an Al target as well as the plasma's spectral emission. The thermal response measurement revealed that the beam refraction occurred since the area of the incident flux was more than twice as large as the laser spot size at the plasma threshold. This effective spot area increased to nine times the actual spot size of the maximum laser flux of 8×10^7 W cm^{-2}. Various methods are employed to estimate the time and space averaged plasma temperature. The LTE thermodynamic diagram indicated an upper limit of 25 000 K based on the air plasma data and the absence of any doubly ionized species of nitrogen or oxygen. The Al emission line ratios yielded a temperature of 12 000 K while the nitrogen lines indicated a temperature of 16 000 K. The difference between the Al and nitrogen line temperatures was attributed to the delayed presence of Al in the plasma volume at which time the plasma had already cooled significantly.

Walters *et al* [3] utilized time resolved emission spectroscopy and various photographic methods to diagnose an Al/air plasma. The paper concentrates mainly on plasma initiation phenomena, laser supported detonation waves in particular. The plasmas are induced with a pulsed CO_2 laser capable of 1.7×10^7 W at peak power.

These early papers and many others [4–6] have indicated that emission spectroscopy is a reliable technique for characterization of LIP. The theoretical background for emission spectroscopy for LIP is described in detail elsewhere [6, 7]. The purpose of this paper is to report the plasma–beam interaction effect during high power CO_2 laser processing of aluminium for a range of powers and speeds. In view of the considerable contemporary interest of laser processing of aluminium alloys, data on the role of plasma on beam absorption and refraction are reported.

2. Experimental procedure

A 10 KW CO_2 laser was used to weld commercially pure Al-1100 alloy and the resultant plasma was studied to understand the physics of the process. All impurities in Al-1100 are below 0.25%. Therefore, it is assumed that impurities will play a minor role in the plasma. The study focuses on the argon plasma for electron temperature calculation. A relative line emission spectroscopic technique is utilized to characterize the plasma in this study. The radiation from a pair of spectral events (lines and/or continuums) is compared as a function of electron temperature. The technique illuminates the need for calibration of the source and is a more straightforward determination of temperature. Key *et al* [8] utilize the laser line technique for the 457.9 and 458.9 nm Ar II line pair in electric arc plasma. Peak temperatures were again in excess of 17 000 K. For our Al metallic plasma studies, the relative line intensity technique was used following the work of Key *et al* [8]. Ar II spectral lines were the result near the centre line and utilized to determine the temperature of this region. The Ar I spectra, which were solvable at a larger radial distance, were used to map this region. The centre line region temperature used to determine the correction factor for the Ar I data and the radiant temperature distribution were subsequently calculated using the absolute intensity of the Ar I spectrum. This technique was used to avoid the error involved in using continual radiation when concentration from spectra other than Ar may be present.

The presence of Al vapour in the Ar/Al plasma appears to drive the experiment towards the LTE states. One realizes that the increased electron number density aids in maintaining LTE while additional evidence is provided by the appearance of Ar II lines in figure 1. Figure 1(*a*) depicts strong Ar I spectral lines along with ionic Ar II lines at 4228 Å, which is not seen in the pure Ar spectra shown in figure 1(*b*). The ratio of the lines and the continuum intensity has been derived [7] as

$$\frac{I_\lambda}{I_c} = 1.3357 \times 10^{20} \left\{ \frac{N T_e^{1/2}}{N_e^2} \right\} \Delta\lambda, \qquad (1)$$

where N = atom number density, N_e = electron number density, T_e = electron temperature, $\Delta\lambda$ = continuum band chosen to be 10 Å and subscripts λ and c indicate the line and continuum properties, respectively.

Using equation (1) and the fact that N and N_e, the functions of T_e, are known, the electron temperature can be found if the intensity ratio is known.

The experimental apparatus is shown schematically in figure 2. The equipment consists of an EG&G optical multi-channel analyser, a detector controller, a two-dimensional SIT vidicon detector, a monochrometer, a servo-motor controller, a personal computer, a filter controller and 3-translation status. The servo-motor control system, which includes a centroid motion controller and an IBM Personal System II computer, has been implemented to control all translation movements simultaneously. The control software is written in Basic and communicates with the centroid motion controller via serial transmissions. This software produces graphical output indicating the laser's focal spot position on the Al sample as well as providing basic motor control. Optical density filters

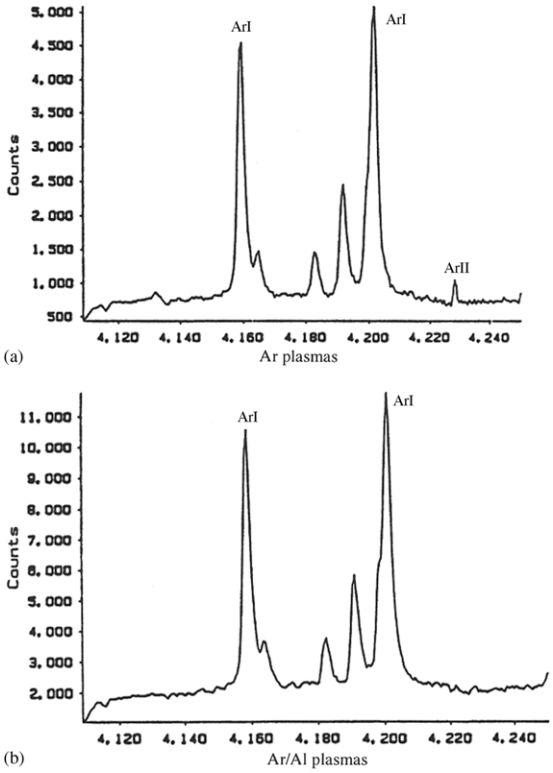

Figure 1. Relative intensity (counts) versus wavelength (Å).

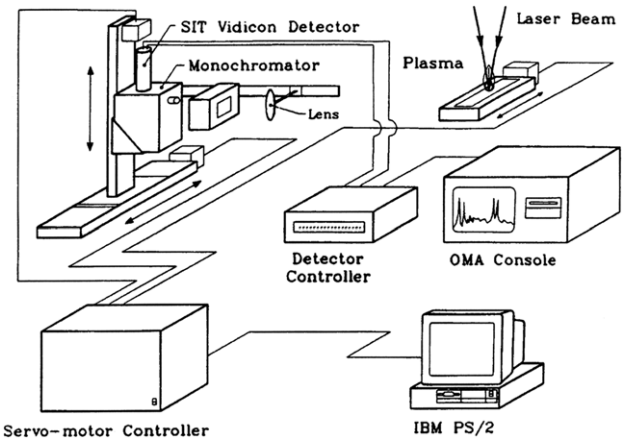

Figure 2. Experimental arrangement for plasma diagnostics.

must be placed in the path of the plasma image to protect the detector face from being burnt by the plasma's intensity. When the Al sample is being irradiated, manual adjustment of the optical filter is impossible, since the geometry of the experimental set-up requires the vidicon detector to be located quite near the 10 kW CW laser. The filter controller is constructed of solenoids, which allow automatic insertion and removal of the various optical filters. The vidicon system was chosen for its relative ease in two-dimensional mapping of plasma parameters. The spectrograph entrance slit was aligned horizontally normal to the plasma axis. The vidicon detector was electronically divided into N-bands or tracks. Each track corresponds to a unique length along the slit. The dimension of the vidicon normal to the slit length corresponds to the wave length. The detector/monochrometer optics system was translated vertically to record a subsequent horizontal slice of the plasma. Typical resolution cell size was on the order of 0.04 mm (slit width) by 0.3 mm (optical magnification and detector resolution). All spectral data acquired in this investigation were obtained using the 1200 groove grating which maintains a dispersion of about 25 Å mm^{-1}. This particular dispersion yields a 250 Å wide spectral dimension at the exit port of the spectrograph.

It should be noted that the measured data are a line of sight integrated value of the local intensity (W cm^2 Sr). To determine the local temperature accurately, the measured intensity had to be deconvoluted into radial emissive powers (W cm^3 Sr). The deconvolution process is known as the Abel inversion, which has received much attention since the classical work of the early 1960s. The particular Abel inversion technique used for this study is described in [7].

The 415.8 nm Ar I metastable line has been used primarily for its separation from the other Ar/Al lines and the availability of the adjacent continuum band. The question of self-absorption is a concern. However, work by Preston [9] has shown the effect of self-absorption metastables in this region of the spectrum to be negligible, particularly in relative line spectroscopic diagnostics.

3. Results and discussion

In order to establish the effect of laser processing parameters on plasma formation, absorption and refraction, a matrix of nine separate plasma cases have been characterized for three different translation speeds and three different laser powers. All experiments were carried out in a stainless chamber with a window for optical access. The chamber was filled with argon slightly above atmospheric pressure to avoid any contamination from the air.

Two-dimensional temperature maps of the plasma are used to produce the plasma volume data. The concentration of aluminum in the lower regions of the plasma is discussed qualitatively as are the percent absorption of incident laser power by the plasma and the depth of penetration within the aluminum samples.

3.1. Temperature distribution

The plasmas encountered in this investigation are typically 25–30 mm in length and about 5–8 mm in diameter. Visual observation indicates that the plasma is shaped like a teardrop. Figure 3 compares two plasma cases for laser power = 7.0 kW and translation speeds of 1.0 and 2.5 mm s^{-1}.

The pressure within the plasma initiation chamber was maintained at a level slightly higher than atmospheric (about 1.1–1.2 atm) for each of the plasmas depicted in figure 3. Upon inspection of figure 3, it is apparent that a smaller core begins to form at or near the surface ($X = 0/0$ and the focal plane of the laser) and expands upwards into a larger core throughout the inner 40–60% of the plasma's volume. The core originates at the surface inside the focal spot of the laser due to the presence of aluminum particles, which increases the local electron number density, which in turn tends to generate a high temperature core region. The highest temperatures to

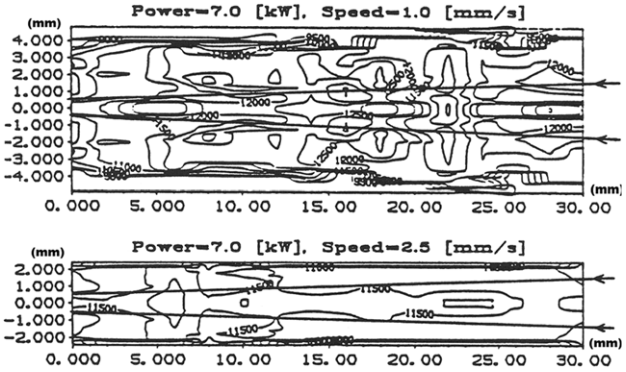

Figure 3. Temperature contours of 7.0 kW plasmas at translation speeds of 1.0 and 2.5 mm s^{-1}.

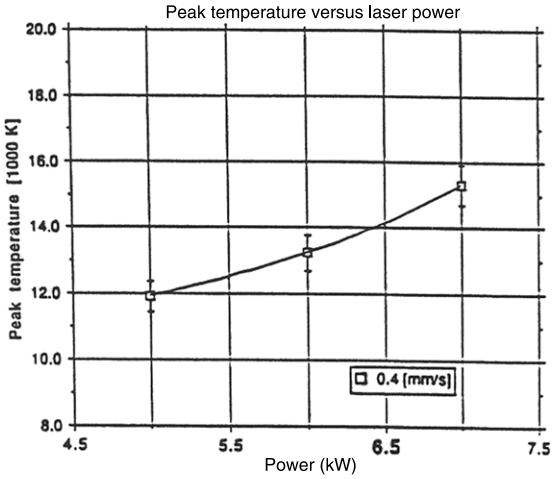

Figure 4. Peak temperature versus laser power for 0.4 mm s^{-1} sample translation speed.

be found in the plasma exist within these cores along the axis of the incoming laser beam. For the plasmas in figure 3, peak core temperatures were on the order of 14 000–15 300 K. An experimental error of ±4% has been applied uniformly across the temperature grid of each plasma [7] and thus applies to the peak core temperatures. This error analysis is designed to predict the 'worst case' scenario.

The peak temperature levels found in each of the plasma cases investigated are shown in figures 4 and 5. While figure 4 seems to be quite predictable, figure 5 reveals an unexpected trend. Figure 4 is based on plasmas induced over the aluminum samples translating at very low speeds. In fact these speeds are low enough that the process could almost be thought of as a stationary drilling procedure. Thus the monatomically increasing nature of the plasma temperature with the laser power for plasmas over low speed samples appears to be expected. On the other hand, the temperature data for plasmas induced over moderate speed samples show (figure 5) a tendency to reach a maximum value of 6.0 kW and then fall somewhat as the power continues to increase. Possible explanations for this trend are as follows: first, the conditions are ripe for a threshold to exist at or around 6.0 kW and above 0.4 mm s^{-1} sample translation speed. Across this threshold, the temperature values of each of the sample speeds appear to decrease at about the same rate even as the laser beam

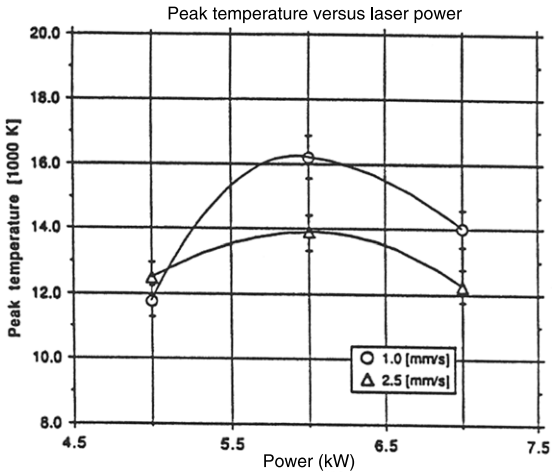

Figure 5. Peak temperature versus laser power for 1.0 and 2.5 mm s^{-1} sample translation speeds.

power is increasing. Possibly involved in this threshold is the increased reflectivity of the plasma as beam power increases, resulting in cooler interior plasma temperatures. Lastly, the chance of data acquisition and reduction systems containing errors is minor. However, the likelihood that these errors would seriously modify the above mentioned trends is quite low. Bearing these facts in mind, the existence of a threshold condition seems to be a very real possibility indeed.

3.2. Power and velocity dependence

The fraction of incident laser power that is absorbed by the plasma has been calculated via the previously mentioned numerical absorption code [7] and is presented here for evaluation. In addition to the absorption data, the beam refraction is determined and used to resolve the final refracted laser beam radius as it meets the sample surface. These variables are compared with the input parameters of the translation speed of the aluminum sample and laser power. The volume of the plasma is also discussed, since it is a function of the power and translation speed and influences other significant variables.

After the spectroscopic data have been acquired, each aluminum sample is examined while typical beam path sites are selected for cross sectioning. The shapes of the melt pool cross-sections are tabulated and presented for discussion.

3.2.1. Absorption. Figures 6 and 7 depict the absorption fraction, or fraction of incident laser power absorbed by the plasma, plotted against the incident laser power. The absorption fraction is calculated for sample translation speeds of 0.4, 1.0 and 2.5 mm s^{-1}. For translation speeds of 0.4 and 1.0 mm s^{-1}, the fraction of absorbed power behaves as expected by increasing as the incident laser power increases. The more intriguing result is the behaviour of the absorption fraction when the sample velocity is 2.5 mm s^{-1}. As indicated in figure 7, the final data point is of interest in that it seems to oppose the trends of the first two curves, and in fact, the trends indicated by each of the previous eight data points.

This point can be better understood by investigating another value of interest, the volume of the plasma. The

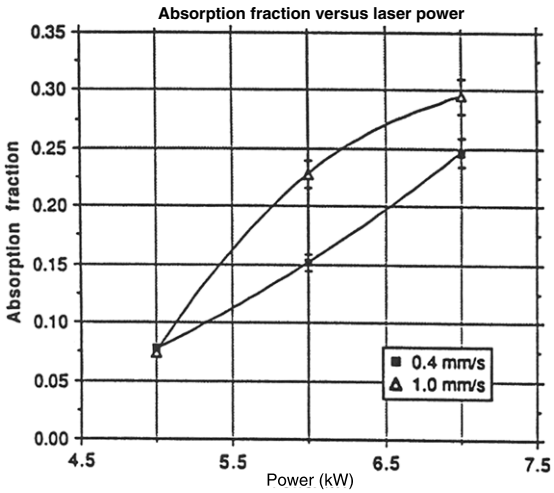

Figure 6. Fraction of absorbed laser power versus laser beam power for translation speeds of 0.4 and 1.0 mm s^{-1}.

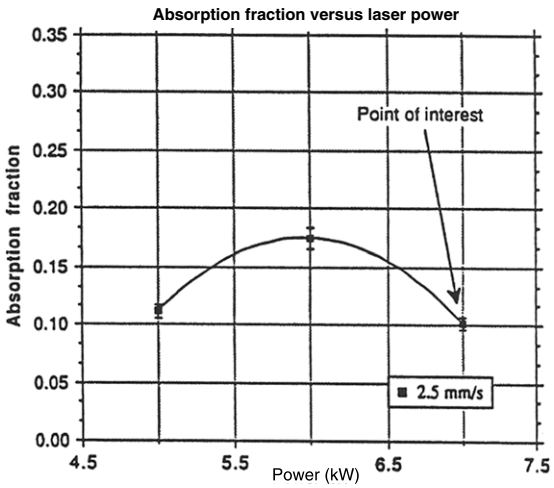

Figure 7. Fraction of absorbed power versus laser beam power for translation speed of 2.5 mm s^{-1}.

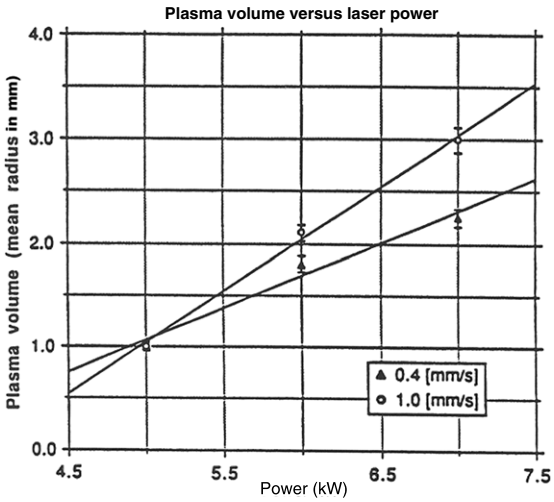

Figure 8. Plasma volume as a function of incident laser power for sample speeds of 0.4 and 1.0 mm s^{-1}.

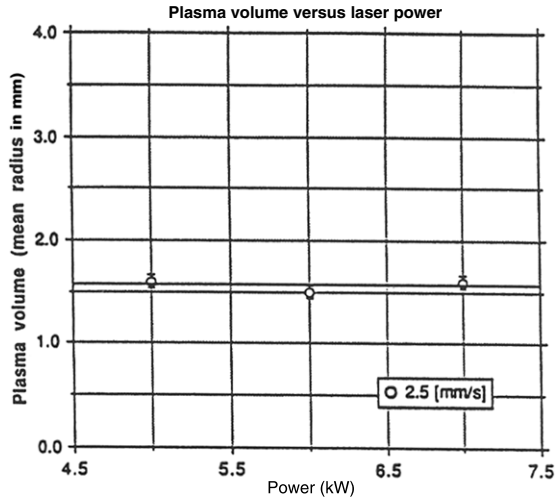

Figure 9. Plasma volume as a function of incident laser power for a sample speed of 2.5 mm s^{-1}.

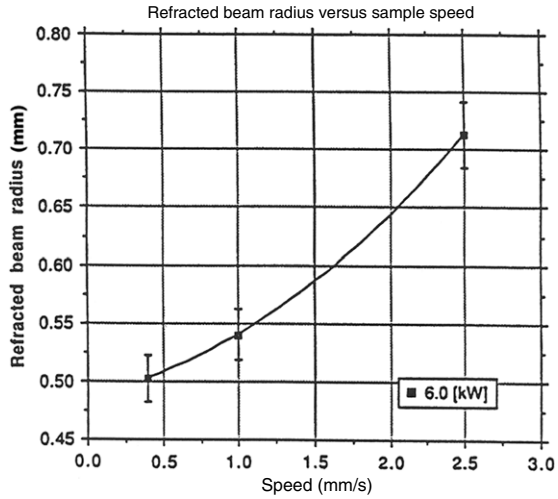

Figure 10. Refracted laser beam radius versus sample translation speed.

volume of the plasma is characterized here by the mean radius of the 11 600 K temperature contour. Figures 8 and 9 characterize the volume of the plasma as a function of the laser power for the three translation speeds. Notice how the trends of the first two translation speeds (figure 8) are very similar: two almost linear increases in the plasma volume as the laser power increases. And, once again, it is evident that the 2.5 mm s^{-1} case (figure 9) is responsible for contesting the trends noticed in the first two curves. Figure 9 portrays a nearly constant plasma volume for the translation speed of 2.5 mm s^{-1}. Considering the experimental errors of ±4% and ±5% for the plasma volume and absorption fraction, respectively, the 2.5 mm s^{-1} curve of figure 9 is not very far from being relatively constant also. Summarizing these trends, it would seem that the absorption fraction is directly proportional to the volume of the plasma.

3.2.2. Refraction. The plasma volume will also tend to affect the refracted beam radius by acting as either a converging or a diverging lens depending on the actual temperature range

of the plasma. The radius of the refracted laser beam as it is projected onto the sample surface is also determined by the aforementioned numerical absorption code [7]. The index of refraction of the plasma is determined as a function of temperature, typically being less than 1.0 for temperatures above 6000 K. The index of refraction has been found to decrease as the plasma temperature increases, consequently refracting the width of the laser beam into a larger spot size on the sample surface. Figure 10 presents the refracted beam radius (mm) of the laser beam at the sample surface versus the translational speed of the aluminum sample. The noteable trend is the increase in the refracted beam radius as the sample speed increases at an incident laser power of 6 kW. One plausible explanation of this trend is that the increased surface refresh rate at the higher translation speed allows a higher concentration of aluminum vapour to reside within the plasma core. The higher aluminum concentration would induce steeper temperature gradients between the core and the outer region of the plasma due to the higher electron number density within the aluminum vapor. Since the index of refraction is inversely proportional to temperature, the steeper temperature gradients of the high speed plasma cases will result in increased laser beam refraction. Figure 10 shows almost a 40% change in the beam radius with increasing traverse speed. For users of lasers for processing, employment of a shielding gas such as 'He' with higher thermal conductivity and ionization potential may be useful to reduce the temperature gradient. A reduced temperature gradient will reduce refraction and thus produce a more effective use of laser energy.

3.2.3. Depth of penetration. The aluminum samples used to induce each plasma case have been examined and representative beam path sites have been cross-sectioned to characterize the shape of the heat-affected zones (HAZ). Each cross-section was cut to an appropriate mounting size and then polished with grit of varying sizes down to and including 0.05 mm alumina powder. The actual microstructures were then accentuated by using Keller's reagent to etch the polished surfaces of the cross-sections. The depth and the width of the melt pool were then carefully measured using an optical microscope.

The width to depth ratio of the melt pool is on the order of 3, verifying that the energy transport mechanism at the surface of the target is conduction dominated with no key-holing occurring in any of the experiments. Further inspection of the cross-sections reveals the presence of what appears to be multiple, embedded melt pools. One possible reason for this fact is that the plasma itself flickers occasionally. If the plasma were to flicker or sputter, the amount of laser power reaching the aluminum surface would fluctuate accordingly, since the flickering plasma would briefly refrain from reflecting and absorbing beam power in its weakened state. This type of power fluctuation at the sample surface could possibly generate the observed melt pool pattern, since the time frame between the random bursts of power reaching the surface might provide enough time for the previous melt pool to solidify, enabling the next burst to initiate the new melt on top of the old solidified pool.

The actual values of the width to depth ratio have been tabulated and are presented graphically in figure 11. The

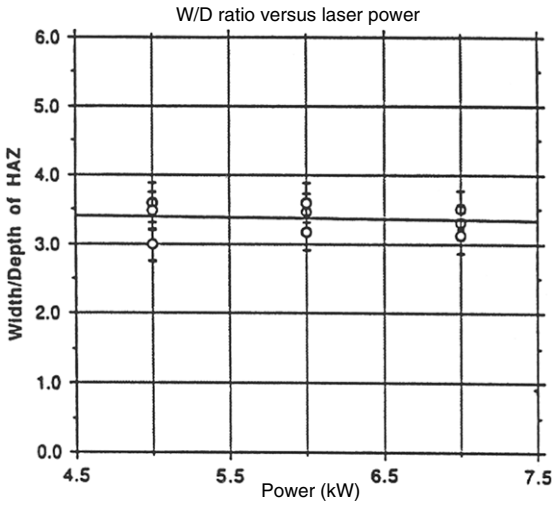

Figure 11. Width/depth ratio of HAZ versus incident laser power.

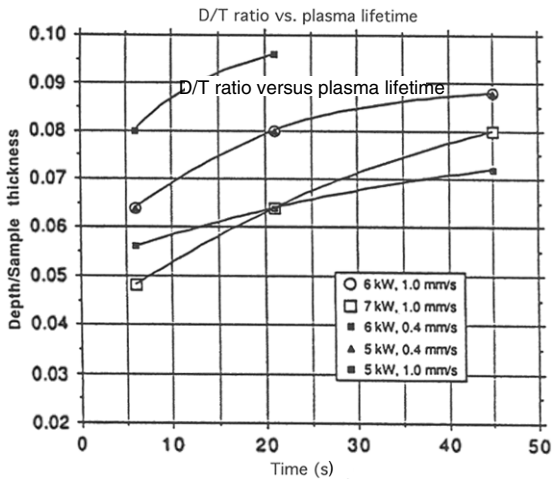

Figure 12. Depth/sample thickness versus elapsed experiment time.

width to depth ratio of each plasma case was relatively constant and fell into the range of 3–3.5 verifying that conduction was the primary energy transport mechanism as mentioned earlier. Figure 12 illustrates the transient effects that come into play with the analysis of the shape of the melt pool.

Several cross-sections were performed for each plasma case, and they were correlated with the time, which passed between the inducement of plasma and their generation. The spatial location of a cross-section on a sample was used with the position logging data from the motion control code to determine the amount of elapsed time from the plasma inducement. Non-dimensionalized with respect to the thickness of the aluminum sample, the depth of penetration is observed to steadily increase as the time of the experiment continues.

The reason behind this behaviour is intuitively obvious: as the experiment progresses, radiation and conduction losses from the plasma as well as the fraction of the laser beam which reaches the sample cause the sample to rapidly approach the melting temperature throughout its mass. Thus the same amount of energy deposited on the sample surface will generate a melt pool at 40 s as at 5 s. This trend is clearly presented in figure 12. It should be mentioned that the relative dimensions

(the overall shape) of the melt pool remained consistent through the duration of the experiment.

4. Conclusions

Data presented in this paper reveal the role of plasma in absorption, refraction and depth of penetration during the laser processing of aluminum.

In summary, the electron temperature distribution and the incident laser power absorption of the plasma have been assessed. Mappings of the electron temperature distributions have been constructed and have indicated the existence of a high temperature, central core that originates at the surface of the sample and propagates outwards and upwards within the plasma boundaries. The peak temperatures of the cores ranged from 14 000–15 300 K. The experimental data indicated that the plasma absorbed between 7.5% and 29% of the incident laser power within the investigated power range 5–6 kW. The volume of the plasma was correlated with the absorption data and experimental trends indicated that a situation of direct proportionality existed between the two parameters. The refracted beam radius can change by more than 40%, for the experimental range presented in this paper. Temperature gradient in plasma is indicated as one of the major variables affecting refraction.

The analysis of the depth of penetration of the laser beam into the aluminum samples has confirmed that the energy transport mechanism is conduction dominated since no key-holing occurred. The primary factor in this assessment is the width to depth ratio of the melt pools consistently maintaining values on the order of 3–3.5.

References

[1] Knudtson J T, Green W B and Sutton D G 1987 The UV-visible spectroscopy of laser-produced aluminum plasmas *J. Appl. Phys.* **61** 4771–80

[2] McKay J A, Bleach R D, Nagel D J, Schriempf J T, Hall R D, Pond C R and Malief S K 1979 Pulsed-CO_2-laser interaction with aluminum in air: thermal response and plasma characteristics *J. Appl. Phys.* **50** 3231–41

[3] Walters C T, Barnes R H and Beverly R E 1978 *J. Appl. Phys.* **49** 2937–43

[4] Fowler M C and Smith D C 1975 Ignition and maintenance of subsonic plasma waves in air by CW CO_2 laser radiation *J. Appl. Phys.* **46** 138–50

[5] Mitchell R W, Conrad R W, Roy E L, Keefer D and Matthews C W 1978 The role of radiative transfer in pulsed laser plasma-target interactions *J. Quant. Spectrosc. Radiat. Transfer* **20** 519–31

[6] Rockstroh T J and Mazumder J 1987 Spectroscopic studies of plasma during cw laser materials interaction *J. Appl. Phys.* **61** 917–23

[7] Rockstroh T J 1986 *PhD Thesis* Department of Mechanical Engineering, University of Illinois, Urbana-Champaign

[8] Key J F, Chan J W and McIlwain M E 1983 *Weld. J.* **62** 1295

[9] Preston R C 1977 *J. Appl. Phys.* B **10** 2381